Supplementary Information (SI) for EES Catalysis.

Electronic Supplementary Information

Anodic activation-mediated formation of crystalline-amorphous heterojunction of CoNi(O)OH for improved urea oxidation activity

Toufik Ansari,[a] Manshu Dhillon,[b] Vijay Patel,[a] Aviru Kumar Basu,[b] Arindam Indra,[a]*

[a]*Department of Chemistry, Indian Institute of Technology (BHU), Varanasi-221005, U.P, India.*
E- mail: arindam.chy@iitbhu.ac.in
[b]*Institute of Nano Science and Technology, (INST), Mohali, India*

Chemicals

All reagents were procured and used without any further purification. Cobalt nitrate hexahydrate (99.9%) was purchased from Sigma-Aldrich. Urea (NH_2CONH_2) was purchased from MERCK Life Sciences Pvt. Ltd. While ammonium fluoride (NH_4F) and $K_2[(Ni(CN)_4]$ were purchased from Sigma Aldrich. Nickel foam was purchased from AXYS technology. Double distilled water was used for all the experiments and electrochemical measurements.

Instruments

The crystallinity and phase of the synthesized catalysts were confirmed by room-temperature X-ray diffraction (Rigaku Miniflex 600) using Cu-K alpha radiation (1.54 Å).

The IR spectra were recorded with the Nicolet iS5 FTIR spectrometer in attenuated total reflection (ATR) mode in the range between 400- 4000 cm^{-1}.

The XPS spectra have been measured using a Thermo Fisher Scientific instrument with Al K-alpha radiation operated at 150 W to study the chemical state of the materials.

The morphology and surface characteristics of the catalysts were examined using a field emission scanning electron microscope (FE-SEM, EVO MA15/18).

Energy-dispersive X-ray (EDX) analysis was performed using the Team Pegasus integrated EDS-EBSD system.

Transmission electron microscopy (TEM) studies were conducted using a Tecnai G2 20 TWIN microscope. For TEM analysis, a small piece of the catalyst film was sonicated in 2 mL of ethanol for 1 hour, and the resulting well-dispersed suspension was drop-cast onto a TEM grid.

Raman spectroscopic (Model: alpha300-RAS) measurements were carried out using a confocal Raman spectrometer.

EPR (Model: EMX-microX) measurements were carried out at low temperature (~93 K).

Activation of nickel foam (NF)

Nickel foam was cut into 1 cm × 2 cm pieces and treated with 3.0 M HCl under ultrasonication to remove the surface oxide layer. After treatment with HCl, nickel foam pieces were washed with water and ethanol repeatedly. The obtained activated nickel foam was dried in an air oven for 6 h at 50 ^oC for further use.

Synthesis

Synthesis of CoNi-CP

1 mmol potassium tetracyanonickelate(II) solution in 25 mL water was added to the solution of cobalt nitrate hexahydrate (1 mmol in 25 mL water) and stirred for 5 minutes. The resulting mixture was kept at room temperature for 24 hours without any stirring. The precipitate was collected via centrifugation, washed with deionized water, and dried in a hot air oven at 60 °C overnight.

Synthesis of NiNi-CP

1 mmol potassium tetracyanonickelate(II) solution in 25 mL water was added to the solution of nickel nitrate hexahydrate (1 mmol in 25 mL water) and stirred for 5 minutes. The resulting mixture was kept

at room temperature for 24 hours without any stirring. The precipitate was collected via centrifugation, washed with deionized water, and dried in a hot air oven at 60 °C overnight.

Synthesis of CoNi-LDH

The CoNi-LDH films were deposited on Ni foam using hydrothermal method. The precursor compounds $Ni(NO_3)_2{\cdot}6H_2O$ (1 mmol), $Co(NO_3)_2{\cdot}6H_2O$ (1 mmol), NH_4F (4 mmol), and NH_2CONH_2 (10 mmol) were dissolved in 12 mL of deionized water. The reaction mixture was stirred at room temperature for 30 minutes and transferred into a 30 mL Teflon cup and a piece of activated nickel foam was kept vertically into the solution. Further, the autoclave was sealed and capped and heated at 120 ^{o}C in an air oven for 5.5 h. As synthesized CoNi-LDH@NF films were washed with water several times and dried at 60 ^{o}C overnight.

Electrophoretic deposition (EPD) of the precatalysts on NF

CoNi-CP and NiNi-CP were electrophoretically deposited onto activated NF in a two-electrode configuration, using NF (2×1 cm^2) as the counter and working electrode in an iodine–acetone mixture. In a typical procedure, 20 mg of the respective material was dispersed in 15 mL of acetone and sonicated at room temperature for 30 min, after which 5 mg of iodine was added and the suspension was further sonicated for 5 min. Immediately thereafter, EPD was carried out at 9 V for 600 s under stirring conditions to obtain uniform catalyst films.

Electrochemical transformation of precatalyst into active catalyst

Cyclic voltammetry (CV) was employed to activate the precatalysts. The activation was carried out in a single-compartment electrochemical cell using CP-loaded NF as the working electrode. Hg/HgO electrode was used as the reference, and a Pt wire as the counter electrode in 1.0 M KOH solution. A scan rate of 5 mV s^{-1} was applied during CV for the anodic activation process.

Electrochemical measurements

Electrocatalytic measurements were conducted in a single-compartment, three-electrode electrochemical cell containing 25 mL of 1.0 M aqueous KOH solution (pH 13.8). The working electrode was the catalyst-loaded NF, paired with a platinum wire counter electrode and a Hg/HgO reference electrode. All electrode potentials were converted to the reversible hydrogen electrode (RHE) scale using the formula:

$E_{RHE} = E_{Hg/HgO} + 0.098 + 0.059pH$

Electrochemical impedance spectroscopy (EIS) was performed over a frequency range of 0.01 to 100,000 Hz with an amplitude of 10 mV. Chronoamperometric (CA) measurements were recorded in 1.0 M KOH at a constant potential without any iR compensation. The Tafel slope was calculated using the standard Tafel equation relating overpotential and current density.:

$\eta = b \log j + a$

Where, η denotes the overpotential (mV), j is the current density (mA cm $^{-2}$), and b is the Tafel slope (mV dec $^{-1}$).

Raman measurement

Raman measurements were performed following a 30-minute chronoamaperometric analysis of the catalyst film by varying the potential. *Operando* Raman spectra were recorded using a confocal Raman spectrometer (Model: alpha300-RAS) with a 532 nm Kr+ ion laser. The laser power at the sample ranged from 0.8 to 2 mW. Throughout the measurements, the film temperature was maintained at 85 K. For the operando experiments, the films were freeze-quenched and stored in liquid nitrogen.

Figures

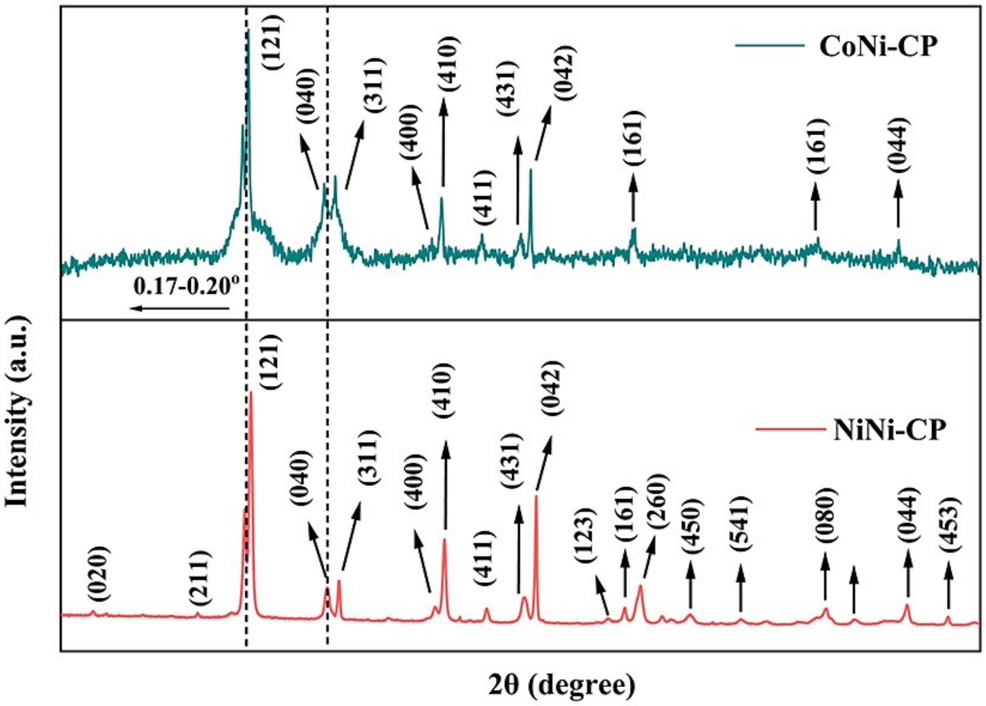

Figure S1. PXRD patterns of CoNi-CP and NiNi-CP. In NiNi-CP, all diffraction peaks are well matched to the Hofmann-type structure $Ni(H_2O)_2[Ni(CN)_4]\cdot xH_2O$.[1-2] In contrast, several peaks in CoNi-CP merged. Moreover, the diffraction peaks of CoNi-CP showed a negative shift of approximately 0.17–0.20° in 2θ compared to to NiNi-CP. [1-2]

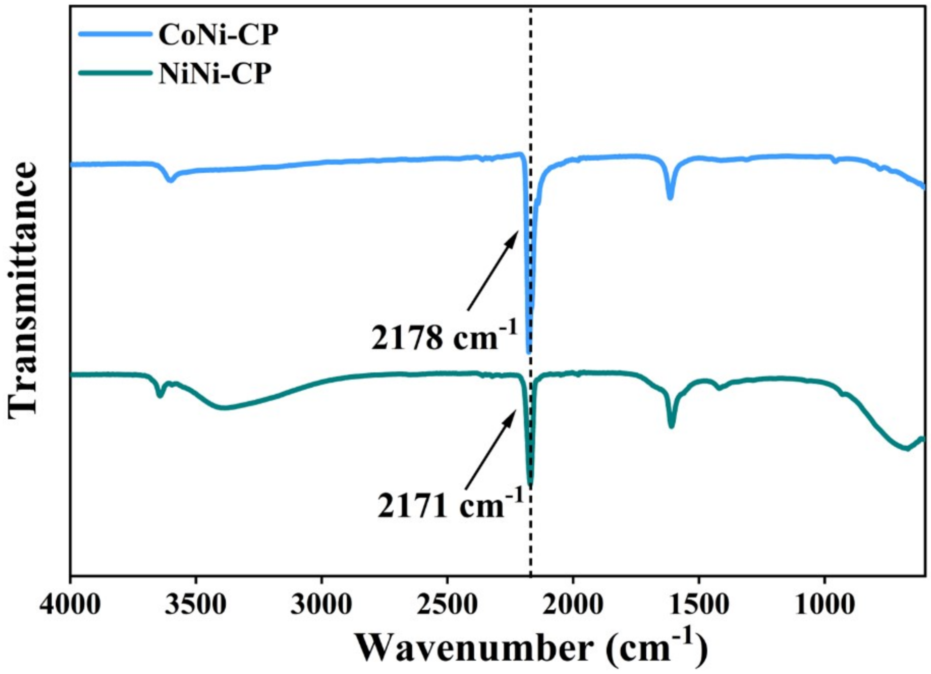

Figure S2. Fourier transformed infrared (FTIR) spectra CoNi-CP and NiNi-CP. [1-2]

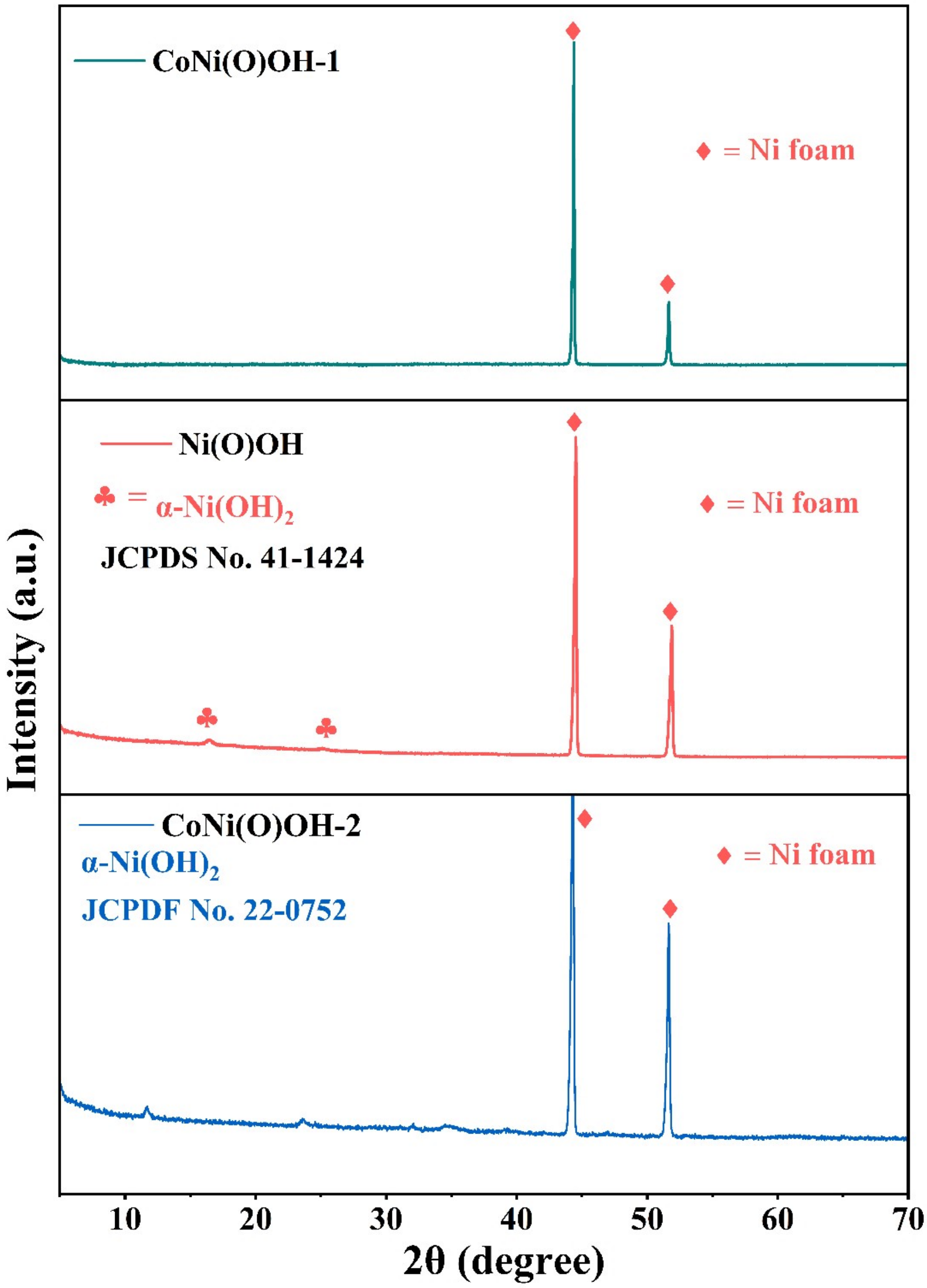

Figure S3. The XRD pattern of CoNi(O)OH-1, CoNi(O)OH-2, and Ni(O)OH after activation.[3-5] The CoNi(O)OH-1 showed amorphous structure, while the CoNi(O)OH-1 was well matched with the α-Ni(OH)$_2$ phase.[3-5] In the Ni(O)OH, a mixed crystalline and amorphous phase was observed.

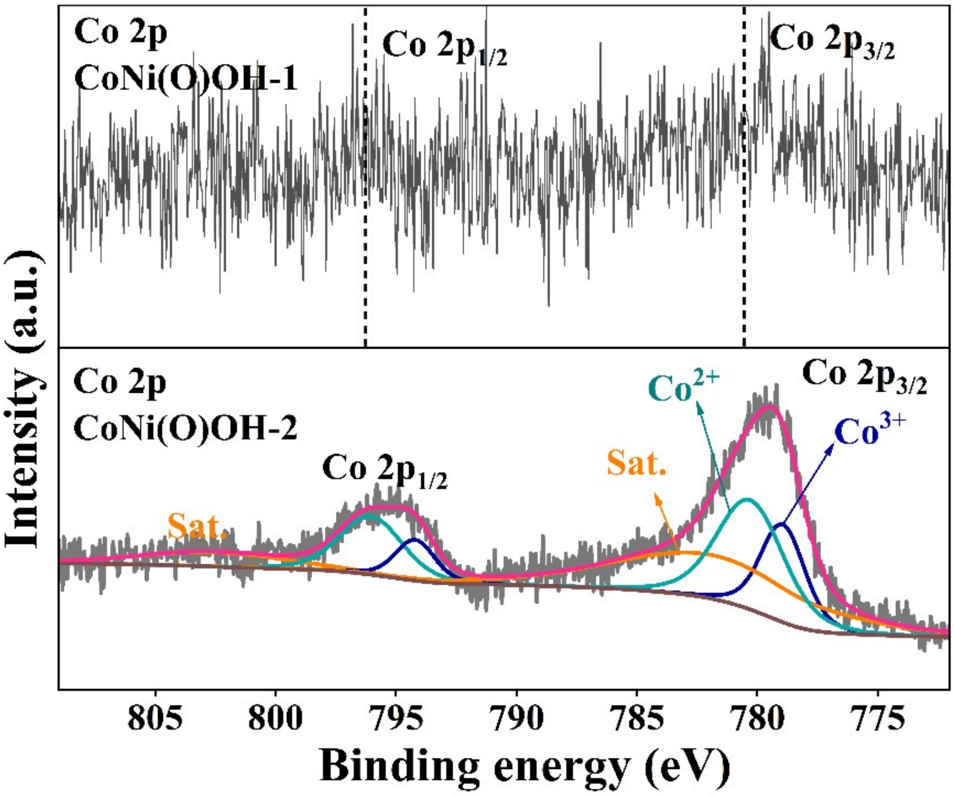

Figure S4. The Co 2p XPS of CoNi(O)OH-1 and CoNi(O)OH-2.[1, 4]

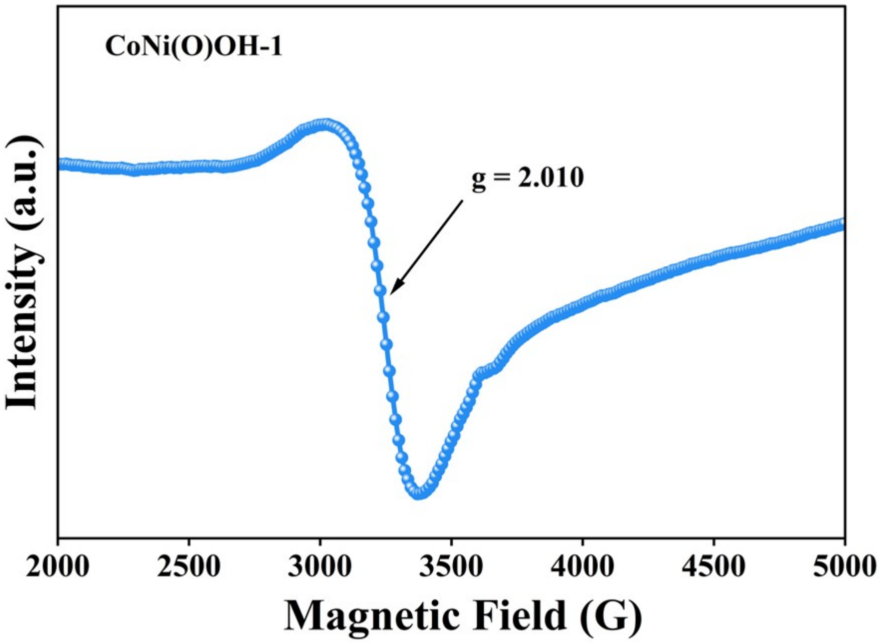

Figure S5. EPR spectrum of CoNi(O)OH-1 at ~93 K.

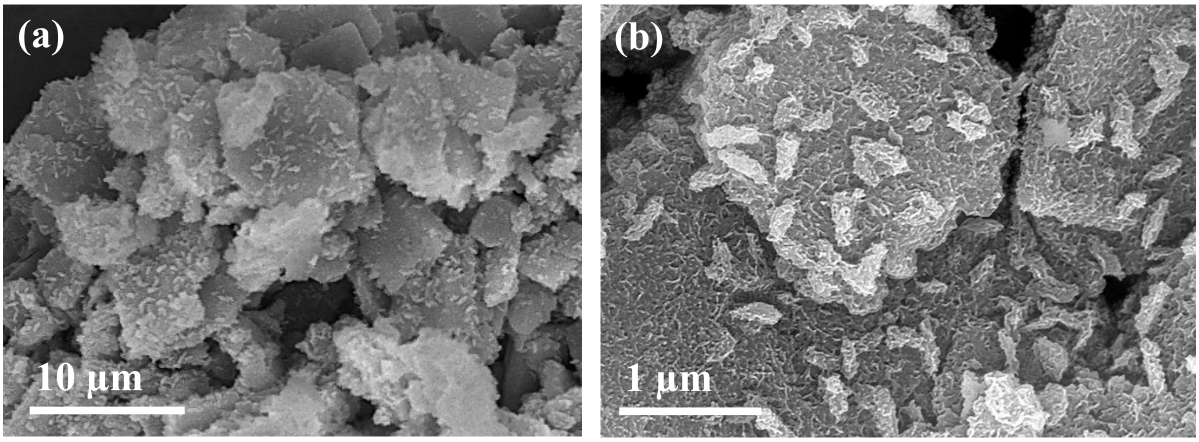

Figure S6. (a-b) SEM images of CoNi(O)OH-1 with different resolutions showing the nanosheet structure.

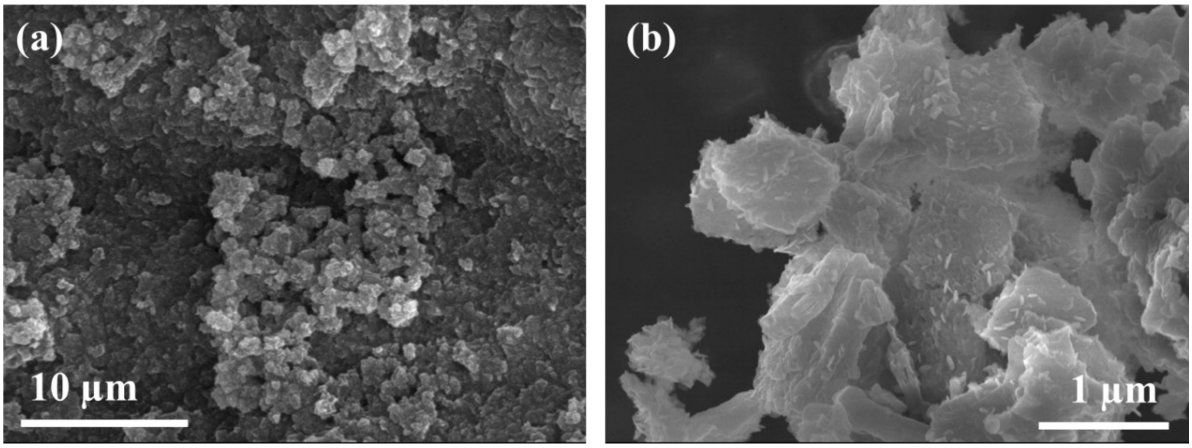

Figure S7. (a-b) SEM images of Ni(O)OH with different resolution showing the nanosheet morphology.

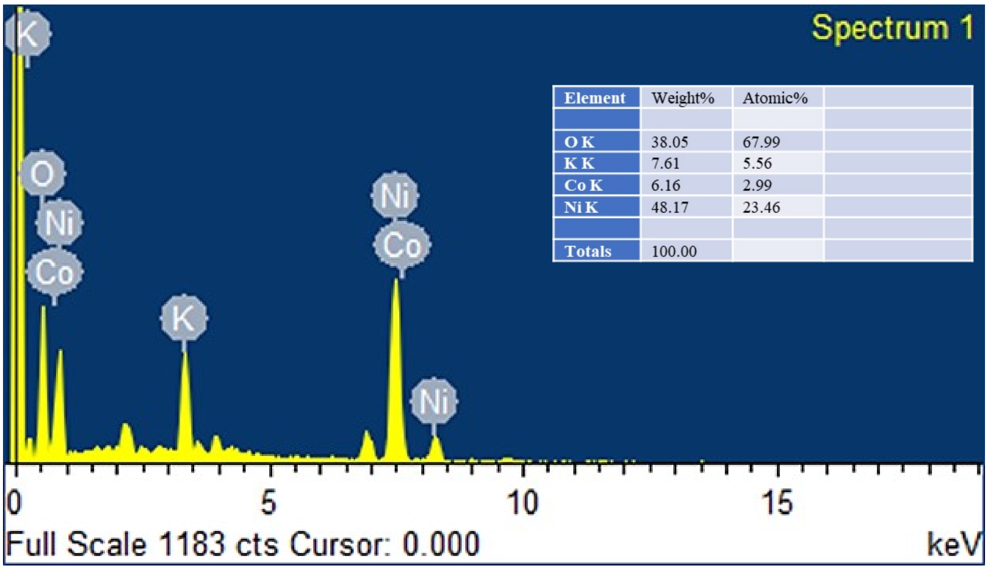

Element	Weight%	Atomic%	
O K	38.05	67.99	
K K	7.61	5.56	
Co K	6.16	2.99	
Ni K	48.17	23.46	
Totals	100.00		

Figure S8. (a) EDX spectrum of CoNi(O)OH-1 shows the presence of Ni, O, and Co. The source of potassium (K) is potassium hydroxide (KOH), which is used as the electrolyte.

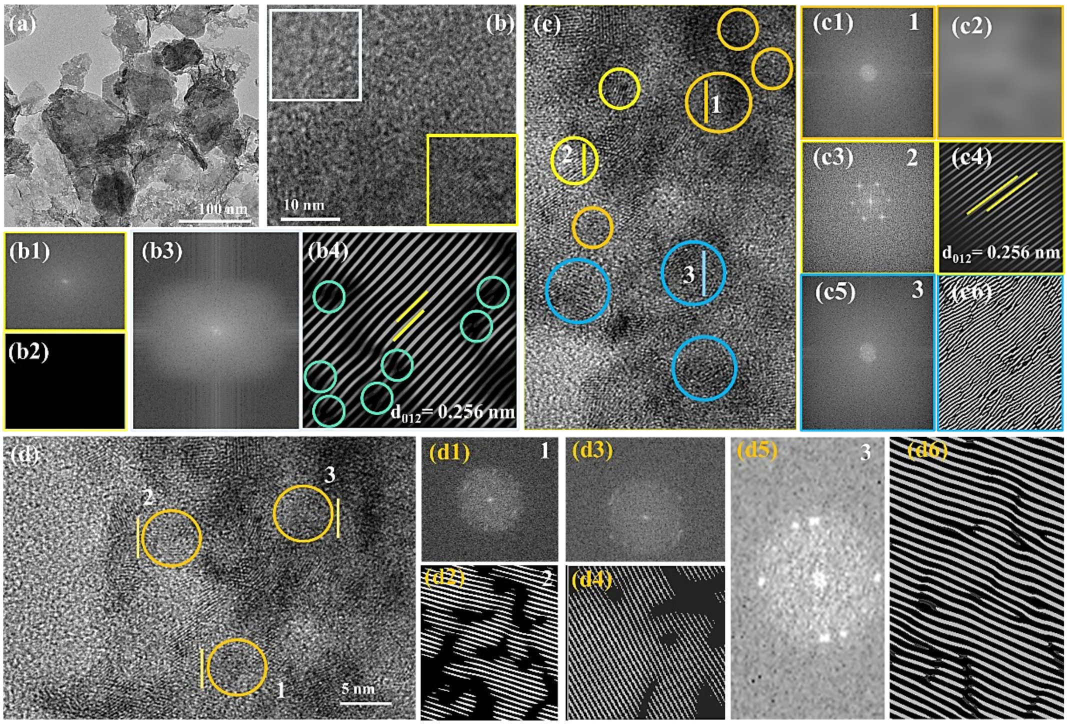

Figure S9. (a-d) TEM image of CoNi(O)OH-1 at different resolutions. (b1–b2) The FFT and IFFT for the yellow-highlighted region in Figure (b) show the absence of lattice rings, confirming its amorphous nature.[7-8] (b3–b4) The FFT and IFFT from the white-highlighted region in figure (b) reveal the clear lattice rings, confirming the existence of a crystalline phase. (b4) The light-green highlighted region indicates the presence of structural disorder. (c1-c2) The FFT and IFFT for the yellow-highlighted region in figure (c) show the absence of a lattice ring, confirming its amorphous nature. (c3–c4) The FFT and IFFT from the circle 2 region in figure (c) reveal the clear lattice rings and fringes, confirming the crystalline phase. (c5–c6) The FFT and IFFT from the circle 3 region in figure (c) show the lattice fringes with a dislocation of the lattice. (d1-d6) The FFT and IFFT attained from the yellow-highlighted circle 1, 2, and 3 regions in figure (d) show the dislocation in the structure.

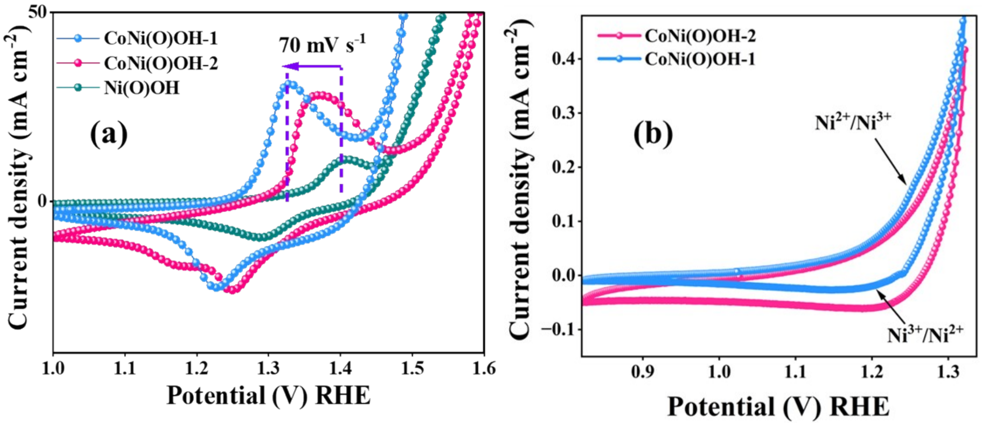

Figure S10. (a) CV profiles of CoNi(O)OH-1, CoNi(O)OH-2, and Ni(O)OH. (b) CV profiles of CoNi(O)OH-1 and CoNi(O)OH-2 in the low-potential region, showing a clear peak for the Ni^{2+} to Ni^{3+} transition in CoNi(O)OH-1, while a broad peak was observed for CoNi(O)OH-2.

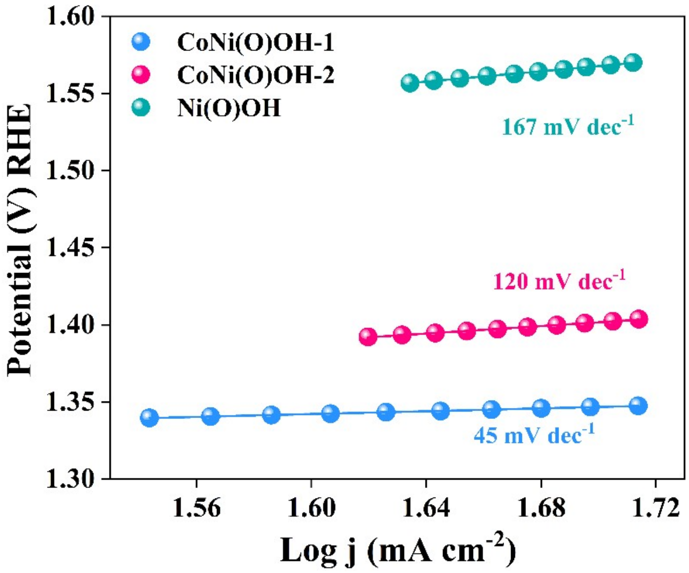

Figure S11. Tafel plots for the active catalysts. The lowest Tafel slope for CoNi(O)OH-1 suggests the fastest OER kinetics.[1-2]

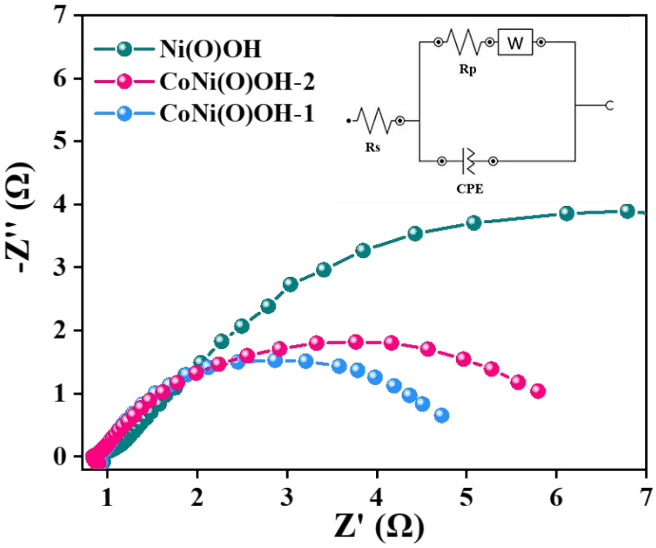

Figure S12. Nyquist plots for the CoNi(O)OH-1, CoNi(O)OH-2, and Ni(O)OH showing the lowest charge transfer resistance for the CoNi(O)OH-1.The frequency range of EIS measurement were 0.01 to 10^6 Hz at 1.5 V *vs.* RHE.

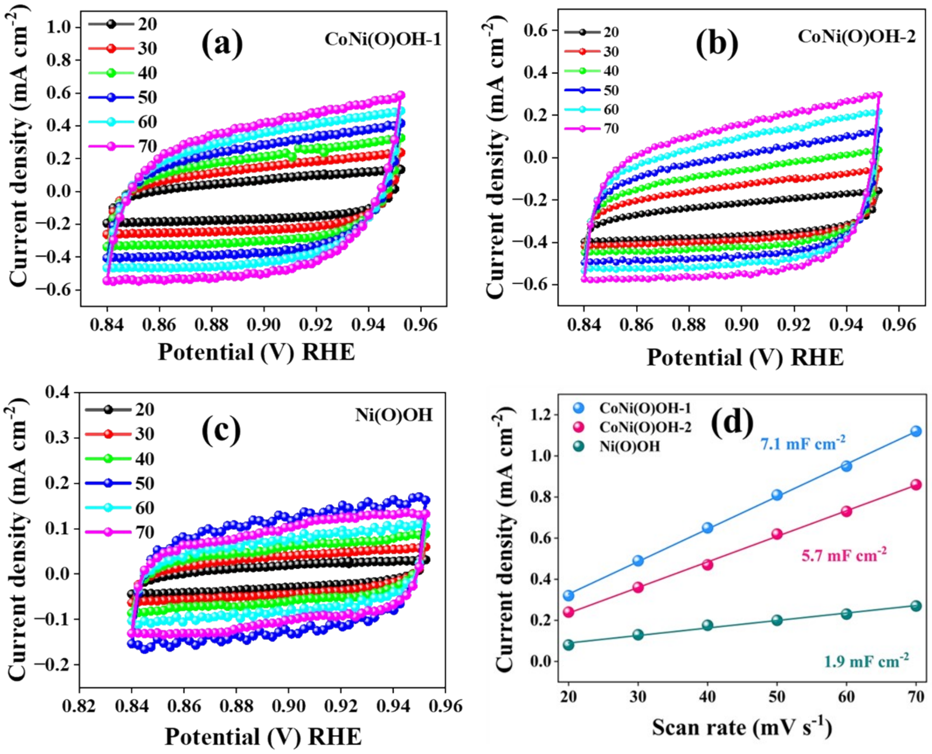

Figure S13. Determination of double-layer capacitance (C_{dl}) of CoNi(O)OH-1, CoNi(O)OH-2, and Ni(O)OH by plotting (difference in the anodic and cathodic current density)/2 against scan rate.[1-2]

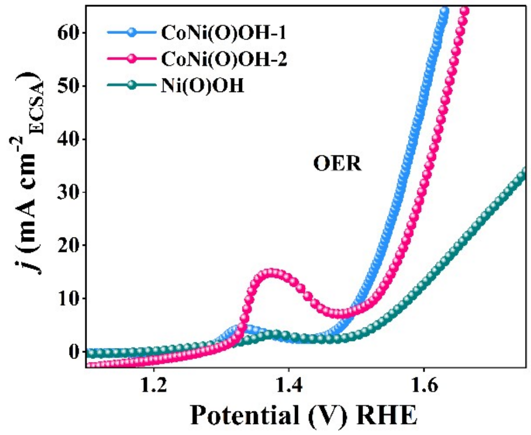

Figure S14. ECSA normalised OER activity of CoNi(O)OH-1, CoNi(O)OH-2, and Ni(O)OH showing the superior performance of the former catalyst.

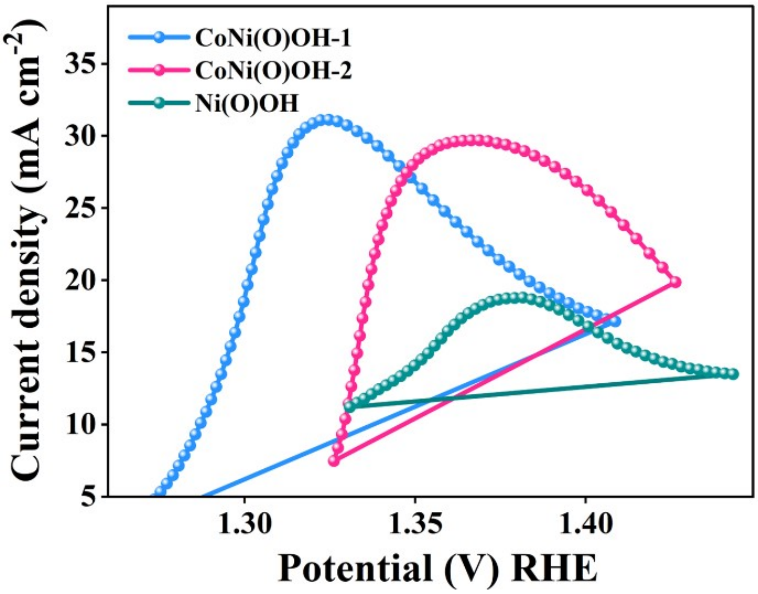

Figure S15. Oxidation peak area used for the active site determination.

Determination of surface active sites using area integration of reduction peak [2]

The ECSA of a catalyst sample is calculated from the double-layer capacitance according to

ECSA = C_{dl}/C_s

C_s = 0.04 mF cm^{-2} in 1 M KOH based on typical reported values.

Where C_{dl} is the double layer capacitance of the catalyst and Cs is the specific capacitance of the material per unit area under identical electrolyte conditions.

For CoNi(O)OH-2

Calculated area associated with the reduction peak = 1.15 x 10^{-6} V A

Hence the associated charge is = 1.15 x 10^{-6} V A / 0.005 V s^{-1}

= 220 x 10^{-3} A s

= 220 x 10^{-3} C

Now, the number of electron transferred is = 220 x 10^{-3} C / 1.602 ×10^{-19} C

= 1.37 x 10^{18}

Since the oxidation of Ni^{2+} to Ni^{3+} is a single electron transfer reaction, the number of electrons calculated above is the same as the number of surface active sites.

Hence,

The surface-active site that participated in OER is = 1.37 x 10^{18}

For CoNi(O)OH-1

Calculated area associated with the reduction peak = 6.802 x 10^{-6} V A

Hence the associated charge is = 1.6 x 10^{-6} V A / 0.005 V s^{-1}

= 330 x 10^{-3} A s

= 330 x 10^{-3} C

Now, the number of electron transferred is = 330 x 10^{-3} C / 1.602 ×10^{-19} C

= 2.06 x 10^{18}

Since the oxidation of Ni^{2+} to Ni^{3+} is a single-electron transfer reaction, the number of electrons calculated above is the same as the number of surface active sites.

Hence,

The surface-active site that participated in OER is = 2.06 x 10^{18}

For Ni(O)OH

Calculated area associated with the reduction peak = 6.802 x 10^{-6} V A

Hence the associated charge is = 0.36 x 10^{-6} V A / 0.005 V s^{-1}

= 72 x 10^{-3} A s

= 72 x 10^{-3} C

Now, the number of electron transferred is = 72 x 10^{-3} C / 1.602 ×10^{-19} C

= 0.4 x 10^{17}

Since the oxidation of Ni^{2+} to Ni^{3+} is a single-electron transfer reaction, the number of electrons calculated above is the same as the number of surface active sites.

Hence,

The surface-active site that participated in OER is = 0.4 x 10^{17}

Since the oxidation of Ni^{2+} to Ni^{3+} is a single-electron transfer reaction, the number of electrons calculated above is the same as the number of surface active sites.
Hence,
The surface-active site that participated in OER is = 0.4 x 10^{17}

Table S1. Comparison of the UOR performance of CoNi(O)OH with previously reported catalysts.

Catalyst	**Catalyst support**	**Electrolyte**	E_{10} (V_{RHE})	E_{100} (V_{RHE})	**Ref.**
CoNi(O)OH-1	NF	1 M KOH + 0.33 M Urea	**1.27**	**1.32**	**This work**
Ni-WO$_x$	NF	1 M KOH + 0.33 M Urea	1.36	1.40	9
O-NiMoP	NF	1 M KOH + 0.5 M Urea	1.31	1.41	10
W-Ni-$C_3S_3N_3$	NF	1 M KOH + 0.33 M Urea	1.36	1.43	11
NiClO-D	GC	1 M KOH + 0.33 M Urea	1.34	1.44	12
P-$CoNi_2S_4$	GC	1 M KOH + 0.5 M Urea	1.31	1.37	13
$Ni(OH)_2$-NiMoO$_x$	NF	1 M KOH + 0.5 M Urea	1.37	1.43	14
CoMn/Co-Mn_2O_4	NF	1 M KOH + 0.5 M Urea	1.32	1.36	15
Cu-NiFe-LDH	GC	1 M KOH + 0.33 M Urea	1.38	1.53	16
Ni-S-Se	NF	1 M KOH + 0.5 M Urea	1.38	1.42	17
Pt-Ni_2P	NF	1 M KOH + 0.33 M Urea	1.36	1.38	18
$IrO_x/Ni(OH)_2$	NF	1 M KOH + 0.33 M Urea	1.34	1.36	19
Co,V codoped NiS_2	CF	1 M KOH + 0.33 M Urea	1.35	1.54	20
O_{vac}-V-$Ni(OH)_2$	NF	1 M KOH + 0.33 M Urea	1.38	1.47	21
NiF_3/Ni_2P	CC	1 M KOH + 0.33 M Urea	1.36	1.57	22
Ce-Ni_3N	CC	1 M KOH + 0.33 M Urea	1.31	--	23
$Cu_{0.5}Ni_{0.5}$ (alloy design)	NF	1 M KOH + 0.33 M Urea	1.33	--	24
$(FeNiCoCrCu)_3O_4$ (alloy)	--	1 M KOH + 0.33 M Urea	1.35	--	25
NiFeSP	NF	1 M KOH + 0.33 M Urea	1.34	--	26
Ni-W_5N_4	NF	1 M KOH + 0.33 M Urea	1.31	1.38	27
CE-NiFe	NF	1 M KOH + 0.33 M Urea	1.32	--	28
$Ni(OH)_2$-NSs	CC	1 M KOH + 0.33 M Urea	1.31	1.41	29
Co_x-$Ni(OH)_2$NPs	CF	1 M KOH + 0.50 M Urea	1.27	1.38	30
Cu:α-$Ni(OH)_2$	NF	1 M KOH + 0.33 M Urea	1.30	1.40	31
NiCoVOx	GC	1 M KOH + 0.33 M Urea	1.29	1.40	32
$Ni_2Fe(CN)_6$	NF	1 M KOH + 0.33 M Urea	1.33	1.35	33
Delithiated $LiNiO_2$	GC	1 M KOH + 0.50 M Urea	--	1.50	34
NiS_2-MoS_2	GC	1 M KOH + 0.33 M Urea	--	1.54	35
$Ni_{1.20}Co_{1.80}O_4$	GC	1 M KOH + 0.33 M Urea	--	1.65	36
Ni@N-doped CNT	GC	1 M KOH + 0.50 M Urea	--	1.60	37
$Ni_{0.85}$Se-on-rGO	CP	1 M KOH + 0.50 M Urea	--	1.60	38

C-NiCo CHs	NF	1 M KOH + 0.33 M Urea	1.145	1.37	39
Fc-NiCo-BDC	NF	1 M KOH + 0.33 M Urea	1.28	1.44	40
NiFe-MIL 53-NH_2	GC	1 M KOH + 0.33 M Urea	1.35	--	41
Ni-MOF 0.5	NF	1 M KOH + 0.33 M Urea	1.35	1.37	42
NiO/Ni	--	1 M KOH + 0.33 M Urea	1.21	--	43
NiO-CrOx	NF	1 M KOH + 0.33 M Urea	1.31	1.40	44
Co-$NiMoO_4$	NF	1 M KOH + 0.33 M Urea	1.30	1.38	45
$NiFe(OH)_X$	NF	1 M KOH + 0.33 M Urea	1.332	1.34	46

[a]NF: Nickel foam; GC, Glassy carbon; CC, Carbon cloth; CF, Carbon fibre.

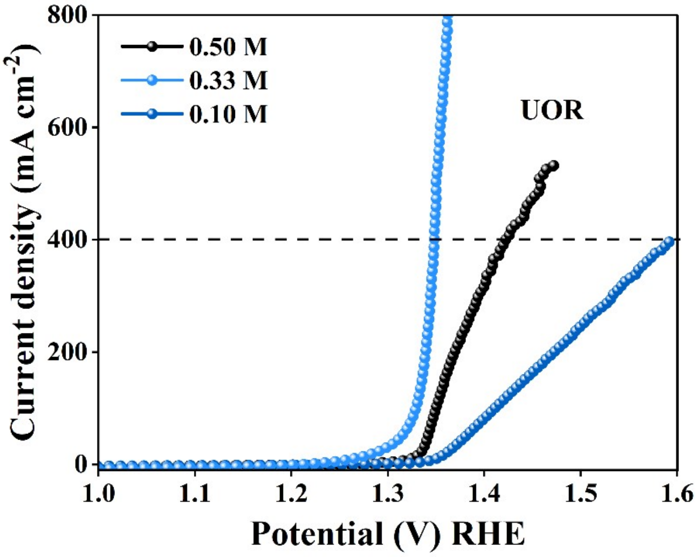

Figure S16. The LSV profile of CoNi(O)OH-1 with varying concentrations of urea, showing the superior activity with a 0.33 M urea concentration.

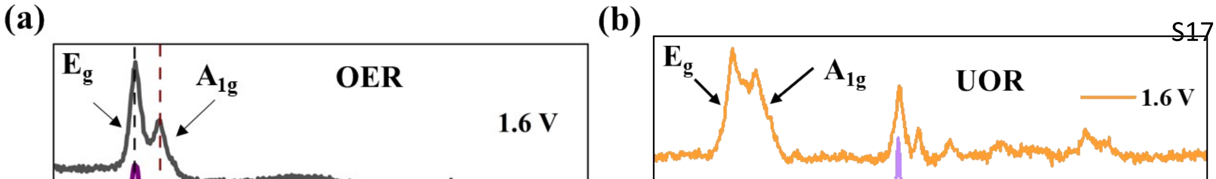

Figure S17. Operado Raman studies during OER and UOR with CoNi(O)OH-1.

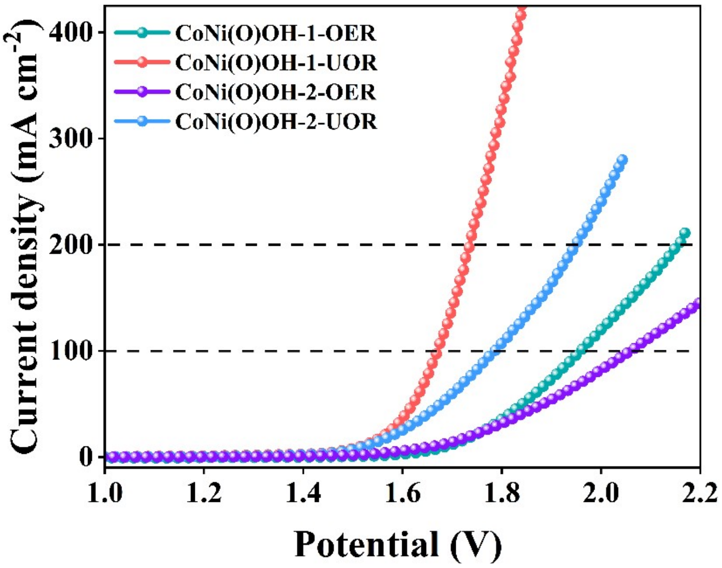

Figure S18. LSV profiles for CoNi(O)OH in a two-electrode system with or without urea (Reaction conditions: 1.0 M KOH + 0.33 M urea at a scan rate of 5 mV s^{-1}).

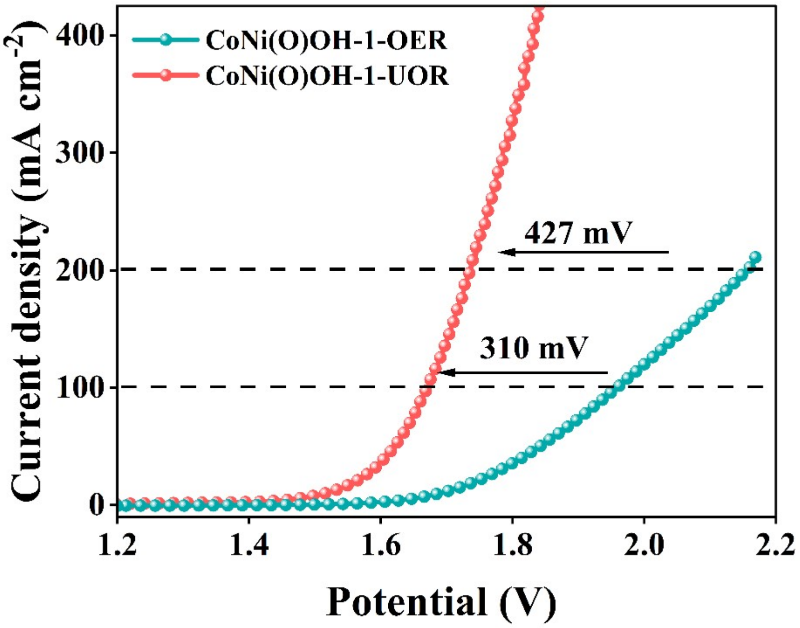

Figure S19. LSV profiles of CoNi(O)OH in a two-electrode configuration with and without urea, demonstrating a 0.310 mV reduction in the applied potential for UOR compared to OER (Reaction conditions: 1.0 M KOH + 0.33 M urea at a scan rate of 5 mV s^{-1}).

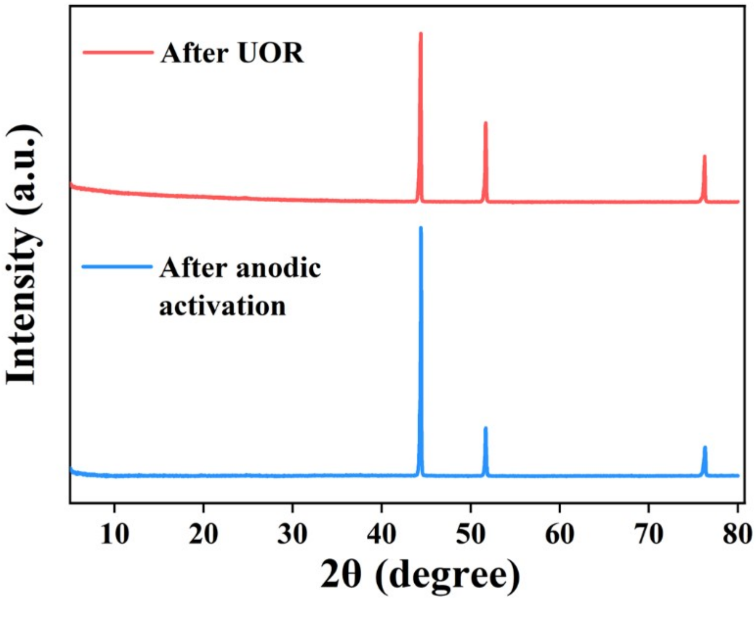

Figure S20. The XRD pattern of CoNi(O)OH-1 after UOR.

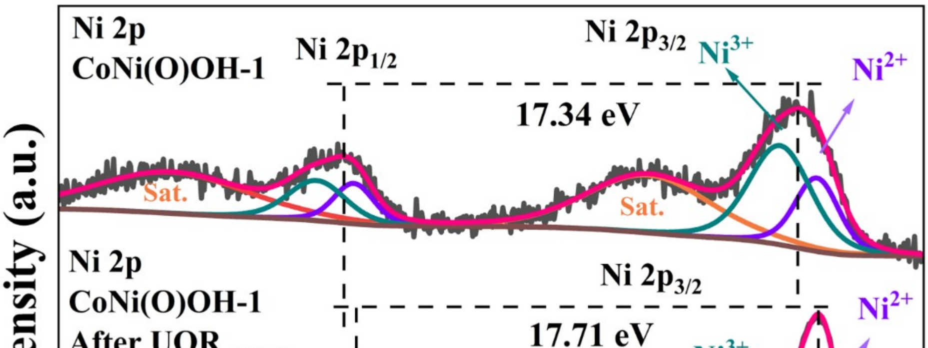

Figure S21. Ni 2p XPS of CoNi(O)OH-1 after UOR. The Ni 2p XPS of CoNi(O)OH-1 after UOR was deconvoluted into two main peaks corresponding to Ni $2p_{3/2}$ and Ni $2p_{1/2}$. The Ni $2p_{3/2}$ region was further split into two peaks for Ni^{2+} and Ni^{3+} species.

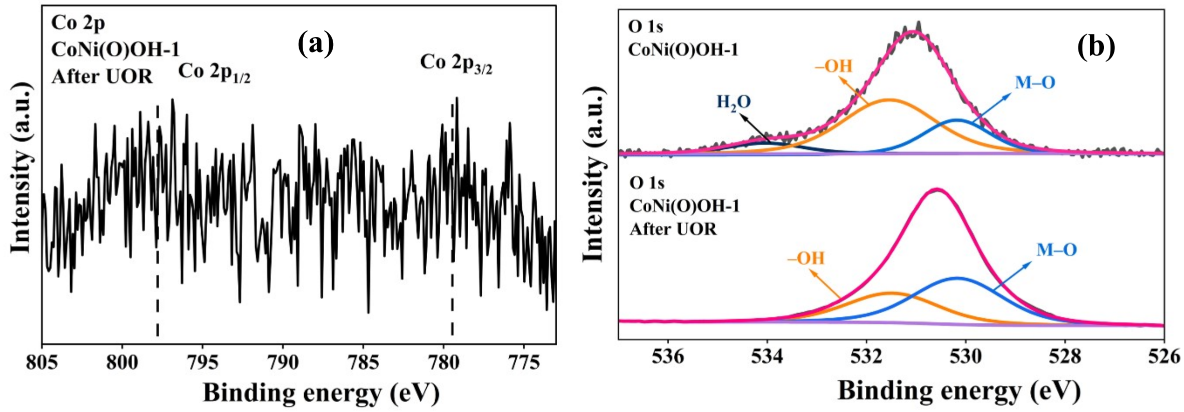

Figure S22. (a) Co 2p XPS of CoNi(O)OH-1 after UOR. (b) The O 1s XP spectrum of CoNi(O)OH-1 after UOR.

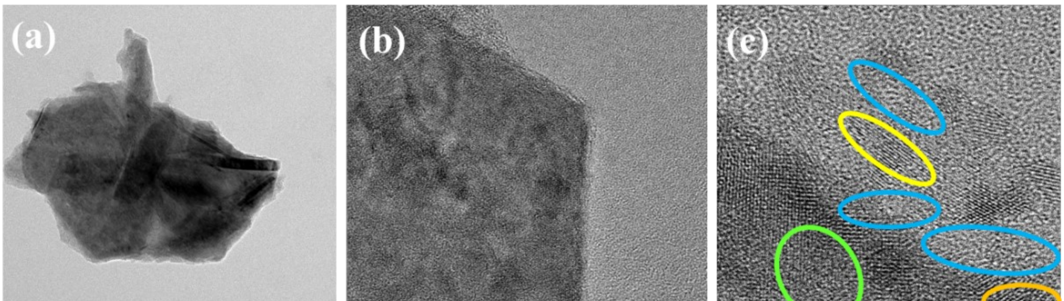

Figure S23. (a-d) The HR-TEM images of CoNi(O)OH-1 after UOR. (d1–d2) The FFT and IFFT for the yellow region and the (d3–b4) golden-yellow region in figure (d) show the lattice fringes of 0.251 nm, corresponding to the (012) plane of the crystalline Ni(O)OH. (d5–d6) The FFT and IFFT of the green region in figure (d) indicate the presence of structural disorder. (d7-d8) The FFT and IFFT for the light blue- region in figure (d) show the absence of a ring, confirming the amorphous nature.

References

[1] X.-Y. Yu, Yi. Feng, B. Guan, X. W. Lou, U. Paik, *Energy Environ. Sci*., 2016, **9**, 1246-1250.

[2] T. Ansari, D. Bagchi, S. Ghosh, J. Niklas Hausmann, A. Indra and P. W. Menezes, *Chem. - A Eur. J.*, 2025, **31**, 202404174.

[3] B. Singh, T. Ansari, N. Verma, Y. C. Huang, P. Mannu, C. L. Dong, A. Indra, J. *Mater. Chem. A,* 2024, **12**, 19321-19330.

[4] J. Du, C. Li, X. Wang, T. G. J. Jones, H. P. Liang, *Electrochim. Acta,* 2019, **303**, 231–238.

[5] Y. Xu, H. Liu, Y. Wu, Q. Wu, C. Li, X. Wang, H. Qin, A. Qin, L. Wang, *ChemNanoMat,* 2023, **9**, 2300414.

[6] Y. Song, X. Wan, Y. Miao, J. Li, Z. Ren, B. Jin, H. Zhou, Z. Li, M. Shao, *Appl. Catal. B,* 2023, **333**, 122808.

[7] L. Jin, R. Ji, H. Wan, J. He, P. Gu, H. Lin, Q. Xu and J. Lu, *ACS Catal.*, 2023, **13**, 837–847.

[8] X. Gao, W. Feng, Z. Zhu, Z. Wu, S. Li, S. Kan, X. Qiu, A. Guo, W. Chen and K. Yin, *Adv. Mater. Interfaces*, 2021, **8**, 2002133.

[9] L. Wang, Y. Zhu, Y.Wen, S. Li, C. Cui, F. Ni, Y. Liu, H. Lin, Y. Li, H. Peng, B. Zhang, *Angew. Chem. Int. Ed.,* 2021, **60**, 10577–10582.

[10] H. Jiang, M. Sun, S. Wu, B. Huang, C-S. Lee, W. Zhang, *Adv. Funct. Mater.,* 2021, **31**, 2104951.

[11] M. Liu, W. Zou, S. Qiu, N. Su, J. Cong, L. Hou, *Adv. Funct. Mater.* 2024, **34**, 2310155.

[12] L. Zhang, L. Wang, H. Lin, H. Y. Liu, J. Ye, Y. Wen, A. Chen, L. Wang, F. Ni, Z. Zhou, S. Sun, Y. Li, B. Zhang, H. Peng, *Angew. Chem. Int. Ed.,* 2019, **58***,* 16820–16825.

[13] X. F. Lu, S. L. Zhang, W. L. Sim, S. Gao, X. W. Lou, *Angew.Chem. Int. Ed.,* 2021, **60**, 22885–22891.

[14] Z. Dong, F. Lin, Y. Yao, L. Jiao, *Adv. Energy Mater.,* 2019, **9**, 1902703.

[15] C. Wang, H. Lu, Z. Mao, C. Yan, G. Shen, X. Wang, *Adv. Funct. Mater.,* 2020, **30**, 2000556.

[16] J. Tang, Z. Li, H. Jang, X. Gu, C. Sun, M.G. Kim, L. Hou, X. Liu, *Adv. Energy Mater.,* 2024, **14**, 2403004.

[17] N. Chen, Y. -X. Du, G. Zhang, W. -T. Lu, F.-F. Cao, *Nano Energy,* 2021, **81**, 105605.

[18] J. Zhang, J. Feng, J. Zhu, L. Kang, L. Liu, F. Guo, J. Li, K. Li, J. Chen, W. Zong, M. Liu, R. Chen, I. P. Parkin, L. Mai, G. He, *Angew. Chem. Int. Ed.,* 2024, **63,** 202407038.

[19] Q. Zheng, Y. Yan, J. Zhong, S. Yan, Z. Zou, *Energy Environ. Sci.,* 2024, **17**, 748–759.

[20] Z. Ji, Y. Song,S. Zhao,Y. Li, J. Liu,W. Hu, *ACS Catal.,* 2022, **12** , 569–579.

[21] H. Qin, Y. Ye, J. Li, W. Jia, S. Zheng, X. Cao, G. Lin, L. Jiao, *Adv. Funct. Mater.,* 2023, **33**, 2209698.

[22] K. Wang, W. Huang, Q. Cao, Y. Zhao, X. Sun, R. Ding, W. Lin, E. Liu, P. Gao, *Chem. Eng. J.,* 2022, **427**, 130865.

[23] M. Li, X. Wu, K. Liu, Y. Zhang, X. Jiang, D. Sun, Y. Tang, K. Huang, G. Fu, J. *Energy Chem.,* 2022, **69**, 506.

[24] K. Zhang, S. Wang, X. Li, H. Li, Y. Ni, *Small,* 2023, **19**, 2300959.

[25] S. L. Fereja, Z. Zhang, Z. Fang, J. Guo, X. Zhang, K. Liu, Z. Li, W. Chen, *ACS Appl. Mater. Interfaces,* 2022, **14***,* 38727.

[26] S. Paygozar, A. S. Rouhaghdam, Z. Li, T. Shao, G. B. Darband, J. Li, *J. Mater. Chem. C*, 2023, **11**, 16074.

[27] Z. Gao, Y. Wang, L. Xu, Q. Tao, X. Wang, Z. Zhou, Y. Luo, J. Yu and Y. Huang, *Chem. Eng. J.*, 2022, **433**, 133515.

[28] M.S. Wu, C.Y. Jao, F.Y. Chuang, F.Y. Chen, *Electrochim. Acta,* 2017, **227**, 210–216.

[29] J.T. Chen, S.Q. Ci, G.X. Wang, N. Senthilkumar, M.T. Zhang, Q.H. Xu, Z.H. Wen, *Chemelectrochem,* 2019, **6**, 5313–5320.

[30] C.B. Sun, M.W. Guo, S.S. Siwal, Q.B. Zhang, *J. Catal.*, 2020, **381**, 454–461.

[31] J.F. Xie, L. Gao, S.S. Cao, W.W. Liu, F.C. Lei, P. Hao, X.Y. Xia, B. Tang, *J. Mater. Chem. A,* 2019, **7**, 13577–13584.

[32] J. Zhang, P. Wang, M. Zheng, R. K. Hocking, Y. Zheng, S.-Z. Qiaoa, *ACS Catal.,* 2025, **15**, 3143–3152.

[33] S.-K. Geng, Y. Zheng, S.-Q. Li, H. Su, X. Zhao, J. Hu, H.-B. Shu, M. Jaroniec, P. Chen, Q.-H. Liu, S.-Z. Qiao, *Nat. Energy,* 2021, **6**, 904–912.

[34] W.-K. Han, J.-X. Wei, K. Xiao, T. Ouyang, Prof. X. Peng, Dr. S. Zhao, Prof. Z.-Q. Liu, *Angew. Chem. Int. Ed.,* 2022, **61**, e202206050.

[35] S. Wang, L. Zhao, J. Li, X. Tian, X. Wu, L. Feng, *J. Energy Chem.,* 2022, **66**, 483-492.

[36] Y. Li, H. Jiang, Z. Cui, S. Zhu, Z. Li, S. Wu, L. Ma, X. Han, Y. Liang, *J. Phys. Chem., C,* 2021, **125**, 9190-9199.

[37] Q. Zhang, F. MD. Kazim, S. Ma, K. Qu, M. Li, Y. Wang, H. Hua, W. Cai, Z. Yang. *Appl. Catal., B: Environ*. 2021, **280**, 119436.

[38] L. Zhao, Y. Chang, M. Jia, J. Jia, Z. Wen, *J. Alloys Compd*., 2021, **852**, 156751.

[39] D. Khalafallah, C. Ouyang, M.J. Zhi, Z.L. Hong, *Chemcatchem* 2020, **12**, 2283–2294.

[40] M. Li, H.C. Sun, J.M. Yang, M. Humayun, L.F. Li, X.F. Xu, X.Y. Xue, A. Habibi-Yangjeh, K. Temst, C.D. Wang, *Chem. Eng. J.,* 2022, **430**, 132733.

[41] S.S. Zheng, Y. Zheng, H.G. Xue, H. Pang, *Chem. Eng. J*., 2020, **395**, 125166.

[42] X.F. Xu, Q.M. Deng, H.C. Chen, M. Humayun, D.L. Duan, X. Zhang, H.C. Sun, X. Ao, X.Y. Xue, A. Nikiforov, K.F. Huo, C.D. Wang, Y.J. Xiong, *Research* 2022, **2022**, 9837109.

[43] Q. Li, S.S. Zheng, M. Du, H. Pang, *Chem. Eng. J*., 2021, **417**, 129201.

[44] X.J. Cao, T.Z. Wang, H.Y. Qin, G.L. Lin, L.H. Zhao, L.F. Jiao, *Nano Res.,* 2023, **16**, 3665–3671.

[45] X.Y. Liu, H.H. Qin, G.X. Wang, Q.J. Li, Q.S. Huang, Z.H. Wen, S. Mao, *J. Mater. Chem. A* 2022, **10**, 16825–16833.

[46] X.L. Yang, Y.W. Lv, J. Hu, J.R. Zhao, G.Y. Xu, X.Q. Hao, P. Chen, M.Q. Yan, *RSC Adv.,* 2021, **11**, 17352–17359.